Continental break-up of the South China Sea stalled by far-field compression

Laetitia Le Pourhiet, Nicolas Chamot-Rooke, Matthias Delescluse, Dave A. May, Louise Watremez, Manuel Pubellier

Continental break-up of the South China Sea stalled by far field compression

Laetitia Le Pourhiet *, Sorbonne Université, CNRS-INSU, Institut des Sciences de la Terre Paris, ISTeP UMR 7193, F-75005 Paris, France

Nicolas Chamot-Rooke, Laboratoire de Géologie, Ecole normale supérieure, CNRS UMR8538, PSL Research University, 75005 Paris, France

Matthias Delescluse, Laboratoire de Géologie, Ecole normale supérieure, CNRS UMR8538, PSL Research University, 75005 Paris, France

Dave A. May, Department of Earth Sciences, University of Oxford, OX1 3AN Oxford, United Kingdom.

Louise Watremez, Univ. Lille, CNRS, Univ. Littoral Côte d'Opale, UMR 8187, LOG, Laboratoire d'Océanologie et de Géosciences, Lille, France

Manuel Pubellier, Laboratoire de Géologie, Ecole normale supérieure, CNRS UMR8538, PSL Research University, 75005 Paris, France

Outcome of decades of two-dimensional modeling of lithosphere deformation under extension is that mechanical coupling between continental crust and the underlying mantle controls how a continent breaks apart to form a new ocean. However, geological observations unequivocally show that continental break-up propagates in the third dimension at rates that do not scale with the rate of opening. Here, we perform three-dimensional numerical simulations and compare them with observations from the South China Sea to show that tectonic loading in the direction of propagation exerts a first order control on these propagation rates. The simulations show that in the absence of compression in that direction, continental break-up propagates fast, forming narrow

continental margins independently of the coupling. When compression is applied, propagation stagnates, forming V-shaped oceanic basins and wide margins. Changes in out-of-plane loading therefore explain the alternation of fast propagation and relative stagnation. These new dynamic constraints suggest that the West-to-East topographic gradient across the Indochinese Peninsula prevented continental break-up propagation through the 1000 km wide continental rift of central and west basin of the South China Sea, until the direction of stretching changed 23 million years ago resulting in bypassing and acceleration of continental break-up propagation.

The relative movement of rigid plates on the sphere is described by rotation around a pole. Assuming that continental break-up occurs after some constant amount of continental extension, the propagation rate of break-up should scale with the gradient of stretching rate along strike. Far from the pole of rotation, the velocity of opening is nearly constant over hundreds of kilometres and the model predicts that break-up should occur almost instantaneously[1] (Figure 1a). Within this theory, V-shaped oceanic basins can form only in the close vicinity of the pole of rotation, where variations in the stretching rate are important (Figure 1b). This scissors opening kinematic[2] model has been reproduced by dynamic experiments[3] and numerical simulations[1]. A consequence of this model is that active shortening and thickening of the crust must be observed in the close vicinity of the propagator (Figure 1b). Yet, several well-documented V-shaped propagators, like the East Basin of the South China Sea[4], or the Coral Sea[5,6], are forming far from the pole of rotation within zones of diffuse continental rifting[7] (Figure 1c).

It is widely accepted that the rheological layering of the lithosphere controls the width and structure of passive margins[8,9,10]. Dynamic models have pointed out that mechanical heterogeneities delay the localisation of deformation at the onset of continental rifting[11,12].

Extrapolating these models to continental break-up stage, it is generally hypothesized that Vink kinematic model[7] (Figure 1c) arises from variation in lithosphere strength. Yet, to date, V-shaped oceanic basins have only emerged from dynamic simulations and experiments using scissor opening, and or, simulations with two offset oceanic basins propagating in opposite direction[13,14]. An alternative explanation is therefore needed to explain the stagnation of uni-directional break-up far from the rotation pole.

3D tectonic loading impacts continental break-up

Assuming that break-up propagation is similar to the opening of cracks in an elastic media, local variations in the rate of propagation are expected with variation in loading[15,16]. Here, we study how a small amount of compression, and/or extension, acting normal to the direction of propagation influences the rate of break-up propagation at lithospheric scale, discarding the local effect of magma supply[17] (see methods). In order to study continental break-up propagation, a lithospheric scale weak zone is place on one side of the models to trigger rapid continental break-up after 10 to 15 Myr of stretching at 20 mm/yr. Three 3D simulations are presented in Figure 2: a reference cylindrical experiment, and two experiments in which a small amount of shortening or stretching is applied in the third dimension.

All these models include a mechanically weak lower crust, which is prone to slow localisation of deformation and favour the development of wide rift structure[8,10,18]. Further details are provided in the supplementary method section. Time evolution of the models in 3D and cross-section are provided in supplementary movies 1, 2 and 3.

After 23 Myr of evolution, the break-up has propagated in the pristine part of the three models. Finite plastic strain outlines the orientation of major faults bounding the passive margin. The passive margins are narrow and symmetric and very little differences in width are observed along strike in the models with zero out-of-plane loading (Figure 2b), or with 2.5 mm/yr out-of-plane

extension (Figure 2c). In contrast, the model with 2.5 mm/yr out-of-plane compression (Figure 2a) shows the formation of a wide continental rift at the front of a V-shaped propagator. The width of the rift increases with distance to the propagator and is bounded by minor strike slip structures that make a 45° angle with the direction of extension.

Surface heat flow at the seafloor serves as a proxy for oceanic domain age[19] and shows that with fast break-up propagation, the angle between the seafloor age and the margin is only a few degrees. On the contrary, owing to the slow propagation of break-up, the model with out-of-plane compression displays a typical V-shaped oceanic propagator with angles of more than 30°.

The location of the tip of the oceanic domain with time has been tracked for the three models (Figure 2d). The models with no tectonic forcing or with out-of-plane extension display a clear linear trend with propagation rates of approximately 150 mm/yr. The rate of propagation in the experiment in compression is not constant and the location of the tip of the oceanic domain with time is best approximated by a square root function, meaning that the propagation scales with $t^{-1/2}$, and rate decreases with $t^{-3/2}$ and tends towards zero. The initial break-up is also found to occur slightly later in the model in compression than in the other two models.

The width of passive margin and continental rift are often interpreted as a proxy for the viscosity of the lower crust[8]. All the models presented here have a weak lower crust and therefore should result in the formation of wide continental rifts, according to the current paradigm in the field[9,10,18,20]. Yet, the width of continental rift produced varies from 360 km to 1000 km (see cross-sections in Figure 2).

In order to evaluate the relative effects of lower crustal rheology and boundary conditions on propagation, we provide the results of two supplementary simulations with a ten times larger lower crustal viscosity. Comparing the amount of crustal thinning (Figure 3) indicates that the rheology of the lower crust indeed influences both the rate of propagation of continental break-

up and the width of passive margin when compression is applied. Yet, in extension, rheological effects are negligible as propagation occurs 10 times faster (150 mm/yr) than the far field plate velocity (15 mm/yr).

Propagation of continental break-up modifies the dynamics of continental rifting because the horizontal strain rate increases at the tip of the propagator together with the viscous stress in the lower crust. This favours localised brittle strain at depth and rapid necking. For the fast propagation cases, this leads to the formation of narrow continental margins in a lithosphere with weak lower crust. For the slow propagation case, the width of the continental rift depends on the strength of the lithosphere.

The South China Sea propagator stalled due to Indochina

The South China Sea (SCS) is the largest area of immerged continental crust in the world. The SCS has all the characteristics of a wide continental rift, but crust is thinner and extension has led to continental break-up[21]. In map view, the width of the passive margin increases from 400 km up to 900 km towards the west[22] as the age of sea floor decreases, an observation that is clearly incompatible with typical scissor opening kinematics (Figure 1b). In the following, geological ages are given in million annum (Ma) to contrast with time that remains in million years (Myr).

From 32 Ma (magnetic anomaly 11) to 23 Ma (7-6b) (Stage 1, Figure 4b), the East SCS sub-basin is the only one that accommodates regional extension by spreading. The North-South opening direction at the time is best described by a pole of rotation located E65/N09, far enough from the SCS to dismiss again the scissor-type model. From anomaly 6a the direction of opening changes by 15°[23] as outlined by the change of orientation in magnetic anomaly in the yellow oceanic domain (Figure 4a). The break-up propagates rapidly (Stage 2, Figure 4b) through the central sub-basin, before stalling for 2 Myr until 20 Ma (6/5e) when the last increment of

propagation (Stage 3, Figure 4) took place. The last recorded magnetic anomaly (5c) marks the end of spreading in the SCS[24,25] at 16 Ma.

Discussing the controversial origin, and end, of opening is beyond the scope of this study, since we focus here on the mechanism of propagation. Our interpretations mainly rely on the relative timing of continental break-up of the three distinct oceanic sub-basins, each associated to a V-shaped propagator, and on the change in the direction of spreading and propagation at a time close to magnetic anomalies 7 or 6b (Figure 4). Both observations are robust[23,25,26].

Our study aims at understanding the dynamics of the wide continental rift which preceded the opening of the central and west sub-basin, outlined in brown on Figure 4b and c. This continental rift formed when the East basin was spreading and propagating slowly (Figure 4a and b, blue spreading phase). Our modelling shows that from 32 to 23 Ma, the simultaneity of active continental rifting over the 1000 km width in the west SCS basin, with spreading in the East SCS, cannot be explained solely by a rheological contrast. The slow propagation of continental break-up during this 9 Myr period (Figure 4a and b, blue) is only compatible in rate with models with out-of-plane compression. On the contrary, the fast propagation periods observed in the central and west basin (Figure 4a and b, yellow and pink) are compatible in rate with the experiments with extensional or no tectonic loading at the front.

From the onset of rifting to 23 Ma, rifting occurs on structures that are perpendicular to the Indochinese Peninsula, as recorded by the magnetic anomaly in the East sub-basin and the abandoned rift branch of the Qiongdongnan basin (Figure 4a). As large topographic gradient can propagate compressive stress over hundreds of kilometers[27,28] and dynamic sandbox experiments have witnessed non-instantaneous continental break-up propagation in presence of topographic gradient[29], we propose that the slow propagation results from the topographic load of Indochina. After the change in regional kinematics, the natural direction of propagation points obliquely to

147 the peninsula. From this moment, continental break-up starts to propagate through central and
148 west basin at rates, which can reach 200 km per Myr, as predicted by models with no out-of
149 plane compression.

150 The structure of the passive margin imaged along a refraction profile that cuts across the
151 West and central SCS displays a series of basins overlying an almost flat Moho[30] (Figure 4c).
152 These basins lay on top of the thinned lower crust region, like in the model displayed in Figure
153 2a. These structures do not form with a stronger lower crust (Figure 3). Therefore, if the
154 differences in width of passive margin from East to West also result from the well-documented
155 change in the nature of the lithosphere[31], our simulations suggest the lower crust should be
156 weaker rather than stronger [11,22] in the West and Central Basin. Yet, the mechanical heterogeneity
157 of the crust in this region[26,31] could well be responsible for the 6/5e stagnation period that our
158 simplistic models do not explain.

159 **Oceanic propagators affect the width of passive margins**

160 The width and architecture of magma-poor passive margins are often used as a proxy to
161 measure the initial effective strength of lithosphere, and particularly, the viscosity of the
162 continental lower crust. Here, we have shown that with cylindrical or tri-axial extension
163 boundary conditions, continental break-up propagates ten times faster than tectonic plate velocity
164 erasing the sensitivity of continental rifting structures on crustal rheology.

165 Furthermore, we also demonstrated that a slight component of shortening applied in the
166 direction of propagation reduces propagation rate of continental break-up to the order of
167 magnitude of plate tectonic velocity. This deceleration of rift propagation is recorded
168 geologically by a V-Shape oceanic basin, which cuts across a continental rift zone. While, we
169 point out the Indochinese Peninsula in the case of the SCS, any large gradient in topography can

cause the formation of V-shaped propagator. In the case of scissor opening, the stretching gradient alone is responsible for the topographic gradient[1].

As continental rifting continues at the front and on the side of the propagator during the phase of stalling, the structural complexity increases at the front of the propagator. When/if propagation resumes due to a change in plate motion or simply continues in slow motion, spreading might well occur on an offset segment as evidenced in models with stronger lower crust. This might well be the case in actively propagating d'Entrecastaux Island propagator[32,33], or in the Central Atlantic[34].

The propagation of continental break-up is frequently neglected in the analysis of passive margin formation. Recent studies which include oceanic propagators [13,14,35,36], together with this study, all contradict the conventional idea that the width and the duration of continental rifting reflects the initial mechanical layering of the lithosphere. In comparison with the initial rheological coupling of the lithosphere, three-dimensional kinematic constraints imposed by oceanic propagators have equal or even greater influence on the width of passive margins.

REFERENCES

1 Mondy, L.S., Rey, P.F., Duclaux, G. & Moresi, L. The role of asthenospheric flow during rift propagation and breakup. *Geology* **46,** 103-106 (2017).

2 Hey, R., Duennebier, F.K. & Morgan, W.J. Propagating rifts on midocean ridges. *J. Geophys. Res.: Solid Earth* ***85,*** 3647-3658 (1980)

3 Molnar, N.E., Cruden, A.R. & Betts, P.G. Interactions between propagating rotational rifts and linear rheological heterogeneities: Insights from three-dimensional laboratory experiments. *Tectonics* ***36,*** 420-443 (2017)

4 Briais, A., Patriat, P. & Tapponnier, P. Updated interpretation of magnetic anomalies and seafloor spreading stages in the South China Sea: Implications for the Tertiary tectonics of Southeast Asia. *Journal of Geophysical Research: Solid Earth* ***98,*** 6299-6328 (1993)

5 Weissel, J. K. & Watts, A. B. Tectonic evolution of the Coral Sea Basin. *J. Geophys. Res.* **84**, 4572-4582 (1979).

6 Bulois, C., Pubellier, M., Chamot-Rooke, N. & Delescluse, M. Successive rifting events in marginal basins: the example of the Coral Sea region (Papua New Guinea). *Tectonics* **37,** 3-29. (2017).

7 Vink, G.E. Continental rifting and the implications for plate tectonic reconstructions. *J. Geophys. Res.: Solid Earth*, ***87,***10677-10688 (1982)

8 Buck, W.R. Modes of continental lithospheric extension. *J. Geophys. Res.* ***96,*** 20161-20178 (1991)

9 Huismans, R. & Beaumont, C. Depth-dependent extension, two-stage breakup and cratonic underplating at rifted margins. *Nature* ***473,*** 74-78 (2011)

10 Brune, S., Heine, C., Clift, P.D. & Pérez-Gussinyé, M. Rifted margin architecture and crustal rheology: Reviewing Iberia-Newfoundland, Central South Atlantic, and South China Sea. *Marine and Petroleum Geology* ***79,*** 257-281 (2017)

11 Van Wijk, J. W. & Blackman, D. K. Dynamics of continental rift propagation: the end-member modes. *Earth and Planetary Science Letters* ***229,*** 247-258 (2005)

12 Brune, S., Corti, G. & Ranalli, G. Controls of inherited lithospheric heterogeneity on rift linkage: Numerical and analog models of interaction between the Kenyan and Ethiopian rifts across the Turkana depression. *Tectonics* ***36***, 1767-1786. (2017)

13 Le Pourhiet, L., May, D. A., Huille, L., Watremez, L. & Leroy, S. A genetic link between transform and hyper-extended margins. *Earth and Planetary Science Letters* ***465,*** 184-192 (2017)

14 Liao, J. & Gerya, T. From continental rifting to seafloor spreading: Insight from 3D thermo-mechanical modeling. *Gondwana Research* ***28,*** 1329-1343 (2015)

15 Courtillot, V. Propagating rifts and continental breakup. *Tectonics* ***1,*** 239-250 (1982)

16 Morgan, J.P. & Parmentier, E.M. Causes and rate‐limiting mechanisms of ridge propagation: A fracture mechanics model. *J. Geophys. Res.: Solid Earth* ***90,*** 8603-8612 (1985)

17 Buck, W.R. The role of magma in the development of the Afro-Arabian Rift System. *Geological Society, London, Special Publications* ***259,***43-54 (2006)

18 Huet, B., Le Pourhiet, L., Labrousse, L., Burov, E. & Jolivet, L. Post-orogenic extension and metamorphic core complexes in a heterogeneous crust: the role of crustal layering inherited from collision. Application to the Cyclades (Aegean domain). *Geophysical Journal International*, ***184,*** 611-625 (2011)

19 Parsons, B. & Sclater, J.G. An analysis of the variation of ocean floor bathymetry and heat flow with age. *J. Geophys. Res.* ***82,*** 803-827 (1977)

20 Buck, W.R., Lavier, L.L. & Poliakov, A.N. How to make a rift wide. *Philosophical Transactions-Royal Society of London Series A: Mathematical Physical and Engineering Sciences* ***357,*** 671-689 (1999)

21 McIntosh, K., Lavier, L., van Avendonk, H., Lester, R., Eakin, D. & Liu, C.S. Crustal structure and inferred rifting processes in the northeast South China Sea. *Marine and Petroleum geology* ***58,*** 612-626 (2014)

22 Hayes, D.E. & Nissen, S. S. The South China sea margins: Implications for rifting contrasts. *Earth and Planetary Science Letters* ***237,*** 601-616 (2005)

23 Sibuet, J.C., Yeh, Y.C. & Lee, C.S. Geodynamics of the South China Sea. *Tectonophysics* ***692,*** 98-119 (2016)

24 Li, C.F. et al. Ages and magnetic structures of the South China Sea constrained by deep tow magnetic surveys and IODP Expedition 349. *Geochemistry, Geophysics, Geosystems* ***15,*** 4958-4983 (2014)

25 Briais, A., Patriat, P. & Tapponnier, P. Updated interpretation of magnetic anomalies and seafloor spreading stages in the South China Sea: Implications for the Tertiary tectonics of Southeast Asia. *J. Geophys. Res.: Solid Earth* ***98,*** 6299-6328 (1993)

26 Franke, D. et al. The final rifting evolution in the South China Sea. *Marine and Petroleum Geology* ***58,*** 704-720 (2014)

27 Bird, P., Ben‐Avraham, Z., Schubert, G., Andreoli, M. & Viola, G. Patterns of stress and strain rate in southern Africa. *J. Geophys. Res.: Solid Earth* ***111,*** B08402 (2006)

28 Stamps, D. S., Flesch, L. M. & Calais, E. Lithospheric buoyancy forces in Africa from a thin sheet approach. *Int. J. Earth Sci.* **99,** 1525-1533 (2010)

29 Ding, W. & Li, J. Propagated rifting in the Southwest Sub-basin, South China Sea: Insights from analogue modelling. *Journal of Geodynamics,* **100,**71-86 (2016)

30 Pichot, T. et al. Deep crustal structure of the conjugate margins of the SW South China Sea from wide-angle refraction seismic data. *Marine and Petroleum Geology* **58,** 627-643 (2014)

31 Pubellier, M., Savva, D. , Sapin, F. & Aurelio, M., Structural Map of the South China Sea; scale 1:3M, Commission for the Geological Map of the World

doi:10.14682/2017STRUCTUSCS. *http://ccgm.org/en/home/183-structural-map-of-the-south-china-sea-9782917310342.html* (2016)

32 Taylor, B., Goodliffe, A., Martiniez, F. & Hey, R. Continental rifting and initial sea-floor spreading in the Woodlark Basin. *Nature* **374,** 534-537 (1995)

33 Taylor, B., Goodliffe, A.M. & Martinez, F., How continents break up: insights from Papua New Guinea. *J. Geophys. Res.: Solid Earth* **104,** 7497-7512 (1999)

34 Nirrengarten, M., Manatschal, G., Tugend, J., Kusznir, N.J. & Sauter, D. Nature and origin of the J-magnetic anomaly offshore Iberia–Newfoundland: implications for plate reconstructions. *Terra Nova* **29,** 20-28 (2017)

35 Allken, V., Huismans, R.S. & Thieulot, C. Factors controlling the mode of rift interaction in brittle-ductile coupled systems: A 3D numerical study. *Geochemistry, Geophysics, Geosystems* ***13,*** Q05010 (2012)

36 Zwaan, F., Schreurs, G., Naliboff, J. and Buiter, S.J. Insights into the effects of oblique extension on continental rift interaction from 3D analogue and numerical models. *Tectonophysics* **693,** 239-260 (2016)

CORRESPONDING AUTHOR:

Material and correspondence should be addressed to Laetitia Le Pourhiet

laetitia.le_pourhiet@sorbonne-universite.fr

Acknowledgements

Maps were realised with GMT, post processing with Paraview. We thank Weiwei Ding and M. Pérez-Gussinyé for their reviews. LLP acknowledge financial support of ERC Advanced

Research Grant RHEOLITH (grant agreement No.290864). DAM acknowledge financial support from (FP7/2007–2013)/ERC (Grant Agreement N° 279925) and the Alfred P. Sloan Foundation through the Deep Carbon Observatory (DCO) "Modeling and Visualisation" project.

Author contributions

LLP designed the experiments, analysed the results of the models and wrote the first draft of the paper.

N.C-R drafted the map, discussed the timing of the anomaly and opening of SCS, MD helped for the comparison with the refraction profile and MP discussed the geodynamic setting and the geological arguments.

DAM set up the solver options to run the numerical code efficiently.

LW discussed the results and participated writing the paper.

The authors declare no competing financial interests

FIGURE CAPTIONS

Figure 1: Continental break-up propagation models and observations. a: Almost instantaneous opening far from the rotation pole. b: Scissor opening close to the rotation pole with associated active thickening at the front of the propagator. c: Sketch of propagator observed to form far from the rotation pole with the same colour code, also known as the Vink kinematic model. Contrary to a and b, this kinematic has never been demonstrated with dynamic experiments or simulations.

Figure 2: Modelling set-up and results in term of margin width and propagation of continental break-up. a, b and c present the results of the simulations 23 Myr after onset of rifting with different boundary conditions in the direction of propagation illustrated on the bottom left corners. The cross-sections bb' represent mantle temperature and crustal geometry overlaid with brittle strain (>50%). Synthetic magnetic anomalies (blue-grey) highlight spreading in the oceanic domain. d: Location of the oceanic propagator tip with time for the three models. Interpretative sketches of structures associated with the two modes of propagation.

Figure 3: Effect of rheology versus tectonic loading. Crustal b-factor reflects the local thinning of the crust on passive margin. On the four maps, the white area corresponds to the oceanic domain. The label "Weak" refers to weak lower crust. These "weak" models are the same as those presented in Figure 2. Results labeled "Strong" use a 10 times larger viscosity in the lower crust. Labels "Compression" and "Extension" refers to the out-of-plane tectonic loading described in Figure 2.

Figure 4: Rifting and spreading history of the South China Sea a: Bathymetry (ETOPO1) projected with pole of opening of stage 1 located E65/N09 (mean pole[25]). Colour of sea floor corresponds to the calendar presented in b and is based on the magnetic anomalies[25] shown as blue lines. The red line represents today's location of the bb' cross section of the compression model (Figure 2a). b: Continental break-up calendar (red arrows) is represented with the same axes as Figure 2d to highlight periods of acceleration and stalling. The red circle indicates the bb' cross-section. c: Interpreted seismic refraction profile[29] with the Moho in white and the base of the upper crust in black. See Methods for more details on the projection and basic reconstruction possibilities.

Methods

Map:

Indochina has not move relative to the north margin of the SCS during the time period considered so rather than proposing an ultimate version of these reconstructions that can be found in a number of papers, we use an oblique Mercator projection with the pole of projection being the mean pole of opening for the time period considered here.

The motion are then straight lines (small circles), just like in the model, and tracking the tip of the propagator or the margins at any time is straightforward: northward margin will not move, while southern margin will move straight. This holds until accretion switches to more SW-NE, i.e. the last propagating phase, which we are not comparing to the model.

Modelling Method:

This study uses pTatin3D[37,38] a highly scalable, massively parallel implementation of the finite element method, which employs an Arbitrary Lagrangian Eulerian discretisation, together with the material point method to solve for stokes flow

(1) $\nabla . (2\eta \mathbf{e}) - \nabla P = \rho \mathbf{g}$.

It is coupled with time (t) dependant heat conservation

(2) $\nabla . (\kappa \nabla T) = \mathrm{D}T/\mathrm{D}t$

through non linear temperature (T) and pressure (P) dependant rheologies, detailed thereafter, as well as temperature dependence of buoyancy

(3) $\rho = \rho_0 (1 - \alpha (T - T_0))$

using Boussinesq approximation, which considers changes in density (ρ) are small enough to approximate conservation of mass by an incompressible flow

(4) $\nabla . \mathbf{v} = 0$,

Where **e** denotes the deviatoric strain rate tensor, **v** the velocity, ρ_0 the specific density at T_0. κ and α are respectively the thermal diffusivity and thermal expansion. Non-linear algebraic solvers are based on PETSc[39] and customized with specific solve options[13,38].

Rheology:

The rheology of the models has been kept to a minimum of complexity, i.e temperature dependence and brittle-plastic transition. In order to capture the brittle plastic transition at high confining pressure, Drucker Prager yield stress is limited by von Misses perfect plasticity at high deviatoric stress following $\tau_y = \min[P\sin\phi + Co\cos\phi, \tau_m]$[40]. Effective viscosity for brittle-plastic behaviour depends on local second invariant of strain rate e^{II} following $\eta_Y = \tau_y / e^{II}$ [41]. In order to simulate plastic wear, the friction (ϕ) decreases linearly from initial value of 30° to a final value of 6° after 30 % of plastic strain[42]. τ_m is set to 200 MPa in the crust and 300 MPa in the mantle. The temperature dependence of the viscous strength of rock is approximated by the Frank-Kamenetskii flow rule $\eta_T = \eta_0 \exp(-T/\theta)$. The parameters η_0 and θ are set respectively to 10^{30} Pa.s and 55.6°C in the mantle, 10^{26} Pa.s and 50°C in the lower crust and 10^{27} Pa.s and 50°C in the upper crust. Strong lower crust model have a lower crust viscosity 10 times larger than weak crust models. The effective viscosity η is the smallest of η_T and η_Y. We did not run model with dislocation creep law. This mode of deformation is however only expected to occur in the lower crust because at warmer temperatures, the mantle is expected to flow by diffusion creep. As we show in Figure 3 that models are only sensitive to lower crustal rheology in compression, we therefore believe that this approximation will not drastically affect our conclusions.

Domain, boundary conditions and initial conditions:

The model domain is 600 km long in the direction of propagation (z) and 1200 km long in the stretching direction (x) and extends to 150 km depth. It is discretised using 128 × 32 × 256 high order stable elements (Q2-P1), leading to spatial resolution of 5 km. Each simulation integrates deformation over a time span of 25 to 35 Myr, which corresponds to □ 2000 time

steps on average. The initial geometry includes three horizontal layers: upper crust (20 km), lower crust (20 km) and mantle (110 km) with reference densities ρ_0 set respectively to 2700, 2800 and 3300 kg/m^3 at T_0 = 0°C. The coefficient of thermal expansion, α in equation 3, is constant and equal to 2×10^{-5} /° for all phases.

The initial geotherm corresponds to half-space cooling model for a thermal age of 300 Myr and a constant thermal diffusivity of 10^{-6} m^2/s. This places the lithosphere-asthenosphere boundary as defined by the 1300°C isotherm at 120 km depth initially. Boundary conditions include symmetrical stretching at $v_{x1/2}$ = 10 mm/yr on the left and right sides, free slip on front boundary enforces the model to be cylindrical close to that side, the back side is either assigned free slip or a shortening/stretching velocity of v_z = ±2.5 mm/yr. Infill of mantle material through the bottom boundary compensates for material leaving and entering through the side wall of the models.

In order to study propagation of break-up, it is necessary to ensure that break-up arise more rapidly on one side of the model. This initial localisation is obtained by ascribing larger amplitude (30% instead of a background value of 3%) of random brittle strain to a volume of 100 × 100 × 120 km located at front of the domain. The deformation in this section of domain is not analyzed in the paper.

Neglecting Magma supply:

It has been proposed that in pristine normally thick lithosphere when the supply of magma is large, i.e. above large igneous provinces, individual dikes might propagate over 1000 km[17], weakening the lithosphere over long distance. Our model neglects these magma supply effects.

Yet, modelling study and data show that if dike propagation is directional at short time scale (days), the polarity of propagation alternates at time scales of ten years or less. Upscaling to the timescale of one time step of our models (20 thousand years), dykes might act as a weakening factor but they would not introduce directionality. At long timescale, propagation of

diking is therefore slaved to the magma supply, which occurs beneath the zone of active necking of the mantle. Our model captures the propagation of these lithospheric weakness zones, which are driven by tectonic stress. The lithospheric column located under the ridge is indeed extremely weak and buoyant due to temperature (see Figure 2). When these highly localised zones of warm mantle material reach the surface, they approximate the mid-oceanic ridges at large scale and influences tectonic stress.

Data availability

The data used for the refraction profile that support the findings of this study are available from the corresponding author upon request. The data used to produce the map are taken from ETOPO1 public database[44], and magnetic anomalies have been digitalized from Briais et al. [25].

Code availability

The code used to generate the numerical simulation[37,38] can be access at https://bitbucket.org/ptatin/ptatin3d. Simulations can be reproduced using model RIFT3D_T with example option file SCS.opts.

REFERENCES

37 May, D.A., Brown, J. & Le Pourhiet, L. pTatin3D: High-performance methods for long-term lithospheric dynamics. In *Proceedings of the International Conference for High Performance Computing, Networking, Storage and Analysis*, 274-284 (2014).

38 May, D.A., Brown, J. & Le Pourhiet, L. A scalable, matrix-free multigrid preconditioner for finite element discretizations of heterogeneous Stokes flow. *Computer Methods in Applied Mechanics and Engineering* ***290,*** 496-523 (2015)

39 Balay, S., et al. PETSc users manual revision 3.3. *Computer Science Division, Argonne National Laboratory, Argonne, IL* (2012)

40 Watremez, L. et al. Buoyancy and localizing properties of continental mantle lithosphere: Insights from thermomechanical models of the eastern Gulf of Aden. *Geochemistry, Geophysics, Geosystems* **14,** 2800-2817 (2013)

41 Lemiale, V., Mühlhaus, H.B., Moresi, L. & Stafford, J. Shear banding analysis of plastic models formulated for incompressible viscous flows. *Physics of the Earth and Planetary Interiors* ***171,*** 177-186 (2008)

42 Lavier, L.L., Buck, W.R. & Poliakov, A.N., Self-consistent rolling-hinge model for the evolution of large-offset low-angle normal faults. *Geology* ***27,*** 1127-1130 (1999).

43 Buck, W. R., Einarsson, P., & Brandsdóttir, B. Tectonic stress and magma chamber size as controls on dike propagation: Constraints from the 1975–1984 Krafla rifting episode. *J. Geophys. Res.: Solid Earth* **111,** B12404 (2006).

44 Amante, C. & B.W. Eakins ETOPO1 1 Arc-Minute Global Relief Model: Procedures, Data Sources and Analysis. NOAA Technical Memorandum NESDIS NGDC-24. National Geophysical Data Center, NOAA. doi:10.7289/V5C827 (2009)

442

443

444

445

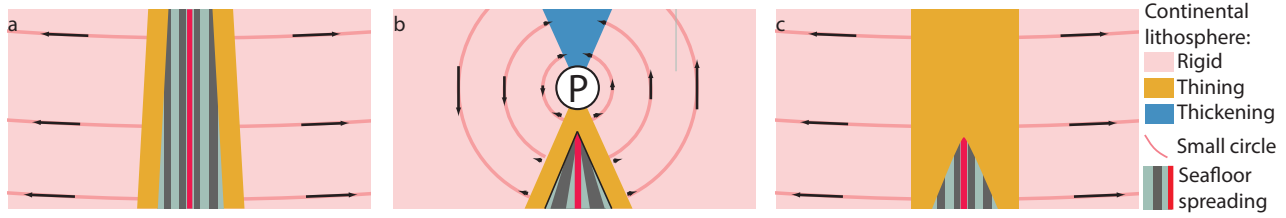
a
b
P
c
Continental lithosphere:
Rigid
Thining
Thickening
Small circle
Seafloor spreading

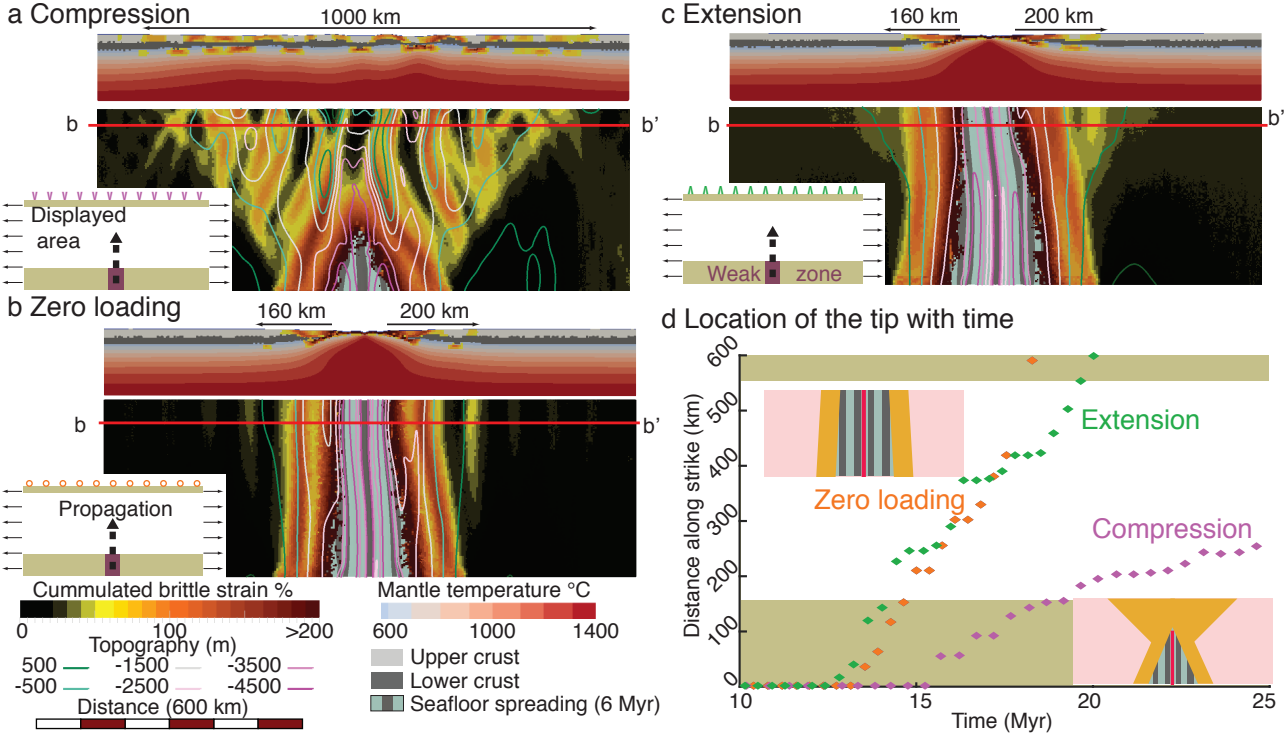
a Compression
1000 km
b
b'
Displayed
area
c Extension
160 km
200 km
b
b'
Weak
zone
b Zero loading
160 km
200 km
b
b'
Propagation
d Location of the tip with time
Distance along strike (km)
Time (Myr)
Extension
Zero loading
Compression
Cummulated brittle strain %
0
100
>200
Mantle temperature °C
600
1000
1400
Topography (m)
500
-500
-1500
-2500
-3500
-4500
Distance (600 km)
Upper crust
Lower crust
Seafloor spreading (6 Myr)

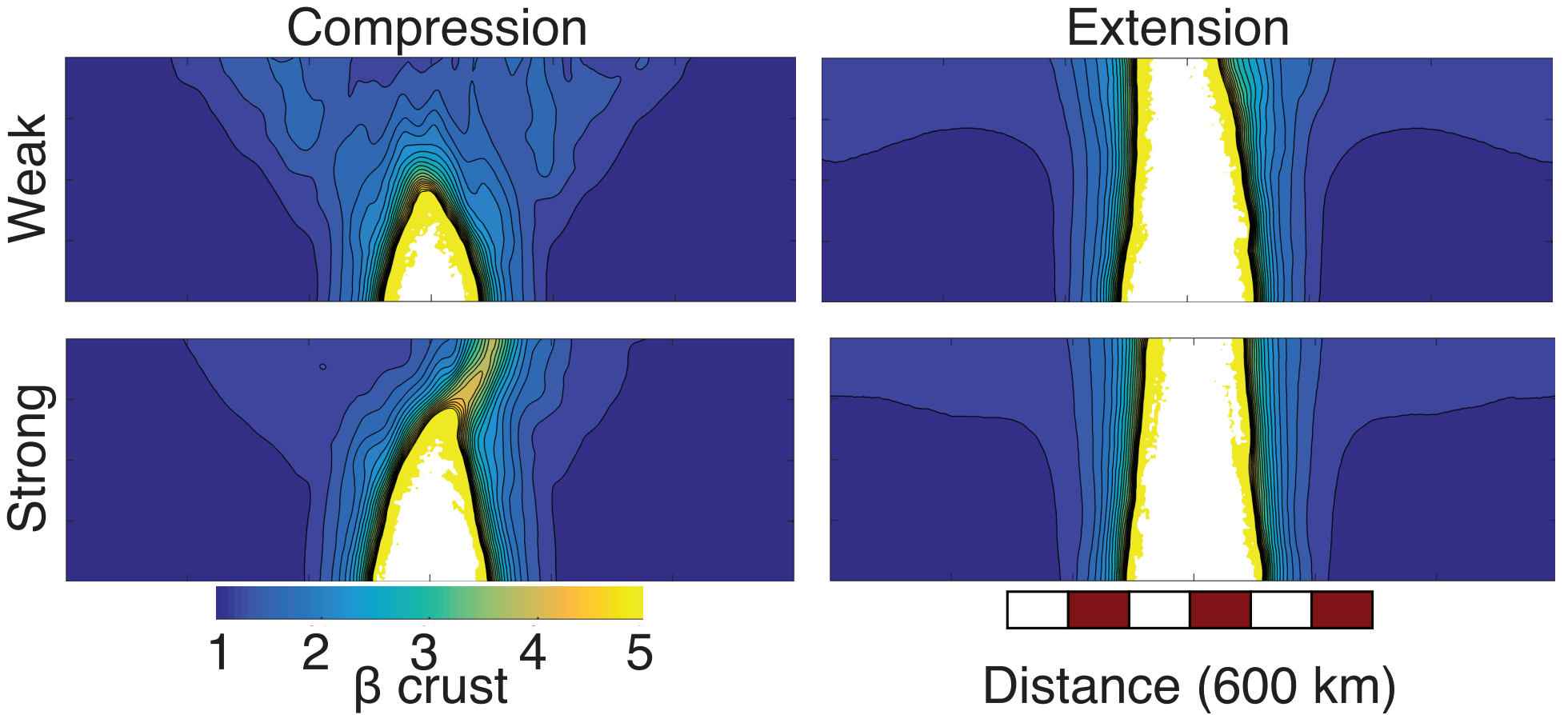
Compression
Extension
Weak
Strong
1
2
3
4
5
β crust
Distance (600 km)

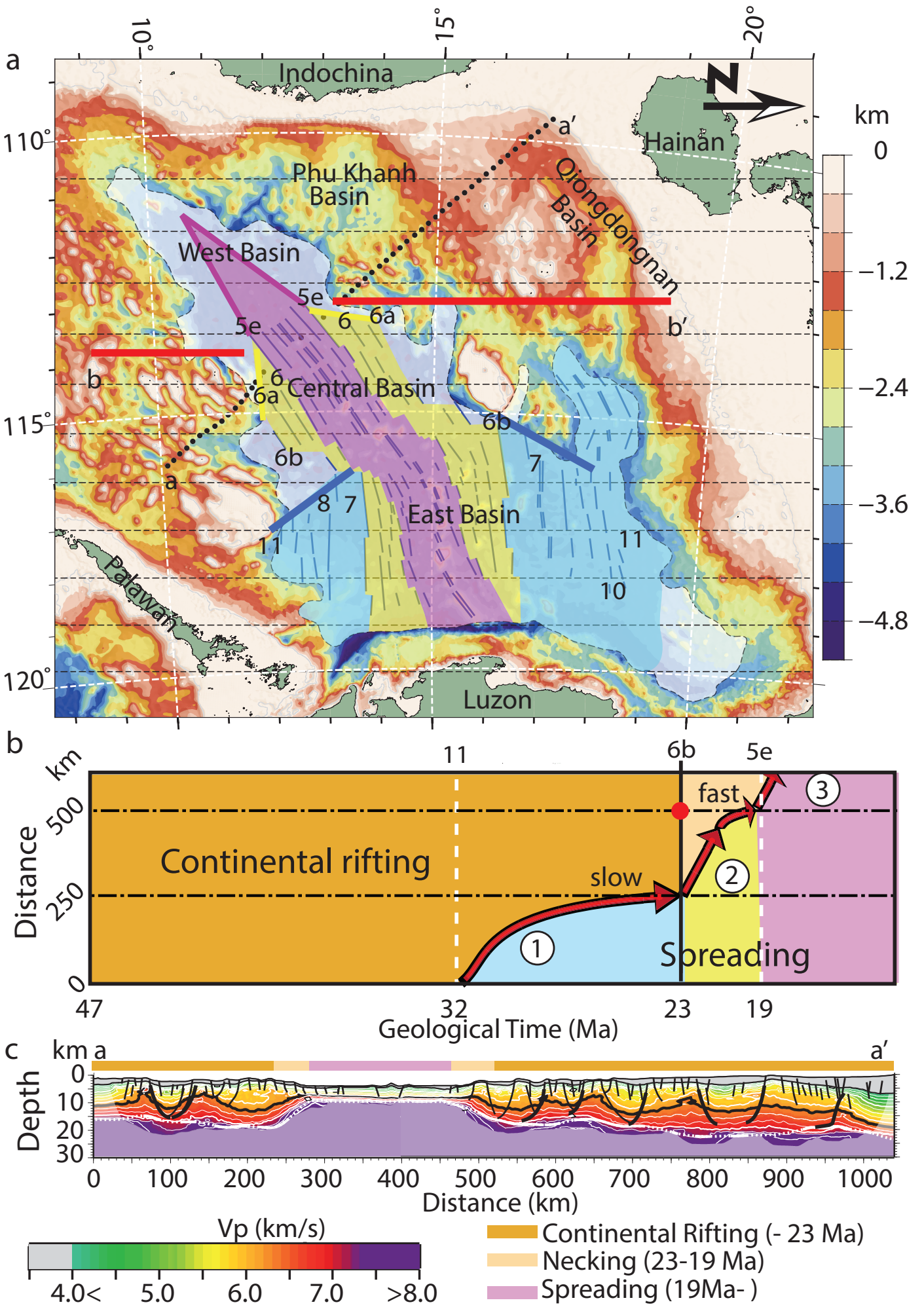
a
10°
15°
20°
110°
115°
120°
Indochina
Hainan
N
km
0
−1.2
−2.4
−3.6
−4.8
Phu Khanh Basin
West Basin
Qiongdongnan Basin
Central Basin
East Basin
Palawan
Luzon
a
a′
b
b′
5e
6
6a
6b
7
8
10
11
b
km
Distance
500
250
0
11
6b
5e
fast
slow
Continental rifting
Spreading
1
2
3
47
32
23
19
Geological Time (Ma)
c
km a
a′
Depth
0
10
20
30
0
100
200
300
400
500
600
700
800
900
1000
Distance (km)
Vp (km/s)
4.0<
5.0
6.0
7.0
>8.0
Continental Rifting (- 23 Ma)
Necking (23-19 Ma)
Spreading (19Ma-)